Structure of the $Al_{13}Co_4(100)$ surface: Combination of surface x-ray diffraction and *ab initio* calculations

É. Gaudry,[1,*] C. Chatelier,[1,2] G. M. McGuirk,[1] L. N. Serkovic Loli,[1,3] M.-C. de Weerd,[1] J. Ledieu,[1] V. Fournée,[1] R. Felici,[4,5] J. Drnec,[4] G. Beutier,[6] and M. de Boissieu[6]

[1]*Institut Jean Lamour, UMR 7198 CNRS Université de Lorraine, 54011 Nancy, France*

[2]*Mines Nancy, Université de Lorraine, 54042 Nancy, France*

[3]*Instituto de Fisica, Universidad Nacional Autónoma de México, Ciudad Universitaria, Coyoacan 04510, Ciudad de México, Mexico*

[4]*ESRF, The European Synchrotron, 71 Avenue des Martyrs, 38000 Grenoble, France*

[5]*CNR-SPIN, Area della Ricerca di Tor Vergata, Via del Fosso del Cavaliere 100, I-00133 Roma, Italy*

[6]*Université Grenoble Alpes, CNRS, SIMAP, F-38000 Grenoble, France*

(Received 29 April 2016; published 10 October 2016)

The structure of the quasicrystalline approximant $Al_{13}Co_4(100)$ has been determined by surface x-ray diffraction (SXRD) and complementary density-functional-theory (DFT) calculations. Thanks to the use of a two-dimensional pixel detector, which speeds up the data acquisition enormously, an exceptionally large set of experimental data, consisting of 124 crystal truncation rods, has been collected and used to refine this complex structure of large unit cell and low symmetry. Various models were considered for the SXRD analysis. The best fit is consistent with a surface termination at the puckered type of planes but with a depletion of the protruding Co atoms. The surface energy of the determined surface model was calculated using DFT, and it takes a rather low value of 1.09 J/m^2. The results for the atomic relaxation of surface planes found by SXRD or DFT were in excellent agreement. This work opens up additional perspectives for the comprehension of related quasicrystalline surfaces.

DOI: 10.1103/PhysRevB.94.165406

I. INTRODUCTION

The intermetallic $Al_{13}Co_4$-type compounds are famous model systems for decagonal quasicrystalline phases. They have been studied extensively in the past few years, both to specify the structure of the various representatives of this family (o-$Al_{13}Co_4$, m-$Al_{13}Co_4$, τ^2-$Al_{13}Co_4$, and o'-$Al_{13}Co_4$) [1–5], whose stability is increased by a proper distribution of vacancies [4,6], but also for their interesting transport and mechanical behavior [7–9]. Most of the applications related to complex intermetallic phases rely on their surface properties. Indeed, these compounds exhibit a low coefficient of friction, low adhesion [10], and high oxidation resistance compared to their metallic constituents [11]. Recently, a few complex intermetallics, among them o-$Al_{13}Co_4$, have also been identified as potential selective catalysts for the semihydrogenation of acetylene [12–15].

A detailed description of their surface structure is a key starting point for understanding the surface properties. While the low-index surfaces of pure metals have been studied for decades and are today well understood [16,17], the surface structure of alloys and intermetallic compounds is much more complex [18]. Surface-science studies of structurally complex intermetallic phases such as quasicrystals and their related periodic approximants emerged in the 1990s with the successful growth of centimeter-sized single crystals and precise crystallographic models [19,20]. Czochralski growth of large single crystals of the $Al_{13}Co_4$ compound was first achieved in 2008 starting from an Al-rich solution [21]. The structure of this complex intermetallic is described as a periodic stacking of two types of atomic planes (flat and puckered) along the [100] pseudo-10-fold direction [2,3] (Fig. 1), or alternatively as a packing of pentagonal bipyramids (Henley-type clusters) [22]. More recently, the existence of a three-dimensional chemical bonding network in this compound has been highlighted by nuclear magnetic resonance (NMR) [23], and theoretical calculations [9] leading to a description of the bulk structure as columns of elongated clusters containing strong Co-Al-Co molecular groups, resembling the three-dimensional "cage-compound" structure of the intermetallic clathrates. Focusing on the surface structure, an important point that is still a matter of debate is the question of the interplay between the three-dimensional bulk structure and the two-dimensional surface.

The o-$Al_{13}Co_4(100)$ surface was investigated recently using a combination of low-energy electron diffraction (LEED), scanning tunneling microscopy (STM), x-ray photoelectron diffraction (XPD), and theoretical calculations based on density-functional theory (DFT). This first study concluded that the surface is bulk truncated, with the selection of puckered atomic planes as termination planes [24]. Further analysis [25,26], using a combination of methods including STM, x-ray photoemission spectroscopy (XPS), dynamical LEED, and DFT calculations, confirmed previous results. In addition, the surface composition deduced from XPS as a function of probing depth below the surface indicated no sign of surface chemical segregation. Surface energy calculations identified four stable surface structures. An agreement between the simulated and experimental STM images was obtained for only two of them, in which all Al atoms of the puckered planes are present but not all Co atoms. Using dynamical LEED analysis, the best agreement was found with a bulk truncated model that consists of Al-rich terminating planes with no Co atoms, and otherwise a structure similar to the bulk puckered layers (selection at the surface of puckered-type

*Emilie.Gaudry@univ-lorraine.fr

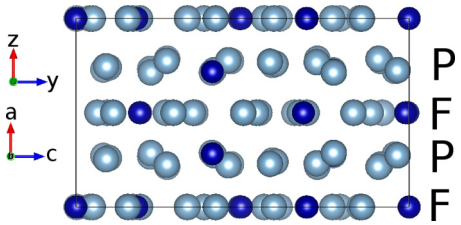

FIG. 1. Bulk structure showing a periodic stacking of two types of atomic planes: flat (F) and puckered (P). Co and Al atoms are represented by dark and light blue, respectively. The cell parameters $a = a_{\text{bulk}}$, $b = b_{\text{bulk}}$, and $c = c_{\text{bulk}}$ are given along with the Cartesian coordinate system (x, y, z) (see Sec. III).

planes). Such a surface structure means that some of the strong bonds of the bulk cluster substructure are broken at the surface. This structure is not compatible with the one deduced from a DFT-based simulated cleavage [13], which corresponds to a surface terminated by an incomplete puckered layer consisting of the tips of one type of the bulk pentagonal bipyramids (Henley-type clusters). Therefore, the $Al_{13}Co_4(100)$ surface structure is still controversial (a dense Al-rich plane built by bulk truncation and a selection of puckered-type planes as surface planes [25,26] versus a highly corrugated surface that preserves the bulk cluster substructure [13]).

So far, experimental studies of complex intermetallic compounds have mainly used conventional surface-science methods. STM images the electronic density of states and provides only indirect information of the surface structure. Elastic and inelastic processes experienced by low-energy electrons ($\simeq$30–300 eV) ensure that the detected diffracted beam intensities are derived entirely from the outermost few atomic layers. However, LEED is dominated by multiple scattering, which implies a demanding data analysis based on a large number of approximations, including nonstructural parameters: spherical atomic potentials, constant inner potential, neglect of the potential barrier at the surface, uniform absorption, and isotropic temperature factors [27,28]. The alternative diffraction method is surface x-ray diffraction (SXRD) [29–31]. In this case, one can generally ignore multiple scattering, which makes data analysis easier. However, the weak interaction between x rays and matter implies some experimental complexity. The latter is performed at synchrotron facilities, under conditions that minimize the scattering contributions from the underlying bulk to ensure surface sensitivity. This technique has already been applied successfully to get insight into the structure of a fivefold quasicrystalline surface (icosahedral $Al_{70.4}Pd_{21.4}Mn_{8.2}$) [32]. Only the specular crystal truncation rod was used, leading to information about the electron density along the z direction only. Using four free parameters (the z displacement and the concentration changes of the last atomic layer, the surface roughness, and a global scale factor), the authors reproduced quite well the measured structure factor. However, drastic assumptions were made—a large number of terminations instead of dense Al-rich layers as topmost layers, for example—severely limiting the confidence in the obtained results.

The objective of the investigation of the $Al_{13}Co_4(100)$ surface structure by *ab initio* calculations and SXRD is to discriminate the different surface models proposed so far, and to solve the exact position of atoms in the near-surface region. This work also demonstrates that SXRD can be used to solve the surface structure of complex intermetallics with large unit cells. This structural determination was possible because of the high density of crystal truncation rods resulting from the large crystal unit cell and the relatively low symmetry of the structure. This, in conjunction with the use of a 2D pixel detector, made it possible for us to acquire the largest experimental data set ever analyzed with SXRD, about five times larger than the next-largest one [33].

The paper is organized as follows. The bulk structure and the surface models are presented in Sec. II. Section III describes the experimental and theoretical methods used in this work. Results are presented in Sec. IV, followed by a discussion and a conclusion in Secs. V and VI, respectively.

II. SURFACE MODELS

The orthorhombic o-$Al_{13}Co_4$ phase crystallizes in the $Pmn2_1$ space group, with the following cell parameters: $a = a_{\text{bulk}} = 8.158$ Å, $b = b_{\text{bulk}} = 12.342$ Å, and $c = c_{\text{bulk}} = 14.452$ Å (Fig. 1). The unit cell contains 102 atoms [2,3], distributed over four atomic planes perpendicular to the pseudo-10-fold direction: sequence $F1P1F2P2$, where the mean position of each plane is 0, 0.25, 0.5, and 0.75, respectively. These atomic planes are represented in Fig. 2 (top view).

In the following, we focus on the pseudo-10-fold surface of o-$Al_{13}Co_4$, perpendicular to the a_{bulk} axis. According to previous studies, the surface plane is found to be derived from the P-type planes only [13,25,26], which present a higher atomic density and a higher concentration of Al compared to the flat planes. In the following, all considered models are built by bulk truncation and selection of the puckered layer as termination planes (Figs. 3 and 4). Only models built from bulk truncation at $P1$ planes ($x_{\text{bulk}} = 0.25$) are shown, but corresponding $P2$ models ($x_{\text{bulk}} = 0.75$) were also included in the SXRD analysis since the surface studied is expected to include both terminations.

Two types of models were built, in agreement with a previous study. The first type presents a complete (or nearly complete) puckered layer as a surface plane, while the second type presents an incomplete puckered layer as a surface plane, in which about half of the surface atoms are absent. The labels for the models are P_i^j, where i is the number of atoms contained in the puckered termination layer, and j indicates the type of atoms present at the surface.

Each complete puckered layer contains four Co atoms per surface unit cell. Two of them are located above the mean position of the puckered layer, while the other two are located below. From this, we have generated four models shown in Fig. 3, which include in the termination plane (i) all four surface Co atoms ($P_{26}^{\text{Al,Co}}$), (ii) only the buried surface Co atoms ($P_{24}^{\text{Al,Co}^-}$), (iii) only the protruding Co atoms ($P_{24}^{\text{Al,Co}^+}$), and (iv) no surface Co atoms (P_{22}^{Al}). All models contain two Al atoms called "glue atoms," located in between the bipentagonal motifs. Their occupancy numbers will be carefully investigated by SXRD.

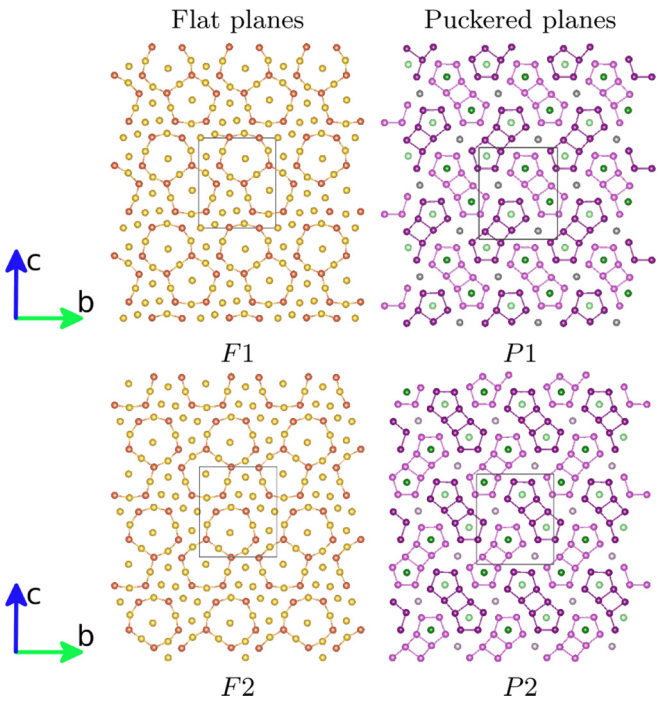

FIG. 2. Atomic planes perpendicular to the [100] direction in $Al_{13}Co_4$. Some atoms have been interconnected so as to show the sections of the pentagonal bipyramids (Henley-type clusters), which are bipentagonal motifs in the puckered plane and bidecagonal motifs in the flat planes. The surface unit cell is shown with black lines: $b_{\text{bulk}} = 12.342$ Å and $c_{\text{bulk}} = 14.452$ Å. In the flat planes, Co and Al atoms are represented by dark and light orange, respectively. In the puckered planes, Co and Al atoms are represented by green and pink, respectively. Atoms slightly below (above) the mean position of the plane are shown by a light color (dark color). Glue atoms in the puckered planes are shown by gray.

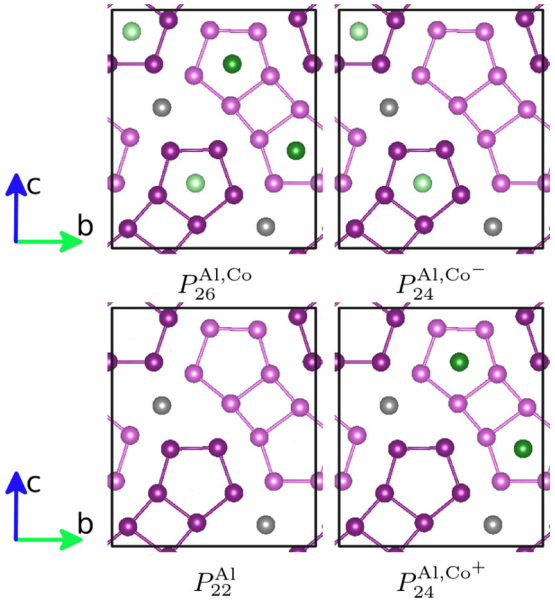

FIG. 3. Surface unit cell of the (almost) complete surface models considered. Co and Al atoms are represented by green and pink, respectively. Atoms slightly below (above) the mean position of the plane are shown by a light color (dark color). Glue atoms are shown by gray.

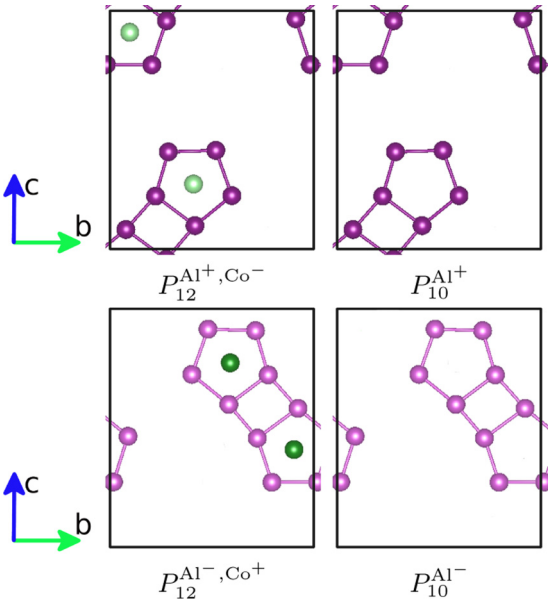

FIG. 4. Surface unit cell of the incomplete surface models considered. Co and Al atoms are represented by green and pink, respectively. Atoms slightly below (above) the mean position of the plane are shown by a light color (dark color).

Figure 4 shows several variations of the puckered termination where only one set of bipentagons is present, described here as an incomplete P-layer model. The motivation for these models came from the STM images, where just one set of the bipentagons was clearly visible. A structure model in which only one set of bipentagonal motifs is present at the surface was also proposed in Ref. [13], resulting from a simulated cleavage experiment. These models do not present surface Al "glue atoms." The considered incomplete models include the one with the bipentagonal motifs containing the top Co atoms ($P_{12}^{\text{Al}^-,\text{Co}^+}$) and the one with the bipentagonal motifs containing the bottom Co atoms ($P_{12}^{\text{Al}^+,\text{Co}^-}$). Variations of these two models are obtained by the removal of surface Co atoms ($P_{10}^{\text{Al}^-}$ and $P_{10}^{\text{Al}^+}$).

III. METHODS

A. Surface x-ray diffraction: Experiment

The x-ray diffraction data were collected at the ID03 surface diffraction beamline of the European Synchrotron Radiation Facility, ESRF, Grenoble. The experimental station (EH2) hosts a z-axis horizontal diffractometer, dedicated to ultrahigh-vacuum (UHV) studies and coupled with a UHV chamber. The x-ray beam was generated by two U35 undulators and was monochromatized with a liquid-nitrogen-cooled monolithic double-bounce Si(111) monochromator. Two mirrors, the first one toroidal with a controllable meridional radius and the second one flat, focused the x-ray beam at the sample position. The incident beam energy was set to 15 keV [34]. The scattered intensity was recorded on a Maxipix area detector.

The $Al_{13}Co_4$ sample used in this experiment was grown using the Czochralski method from Al-rich solutions. Further details are given in Refs. [25,26]. The clean surface was

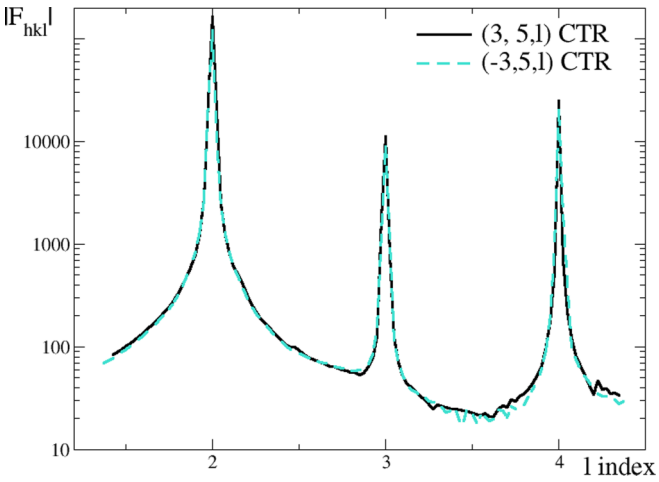

FIG. 5. Module of structure factors $|F_{35}(\ell)|$ and $|F_{-35}(\ell)|$ obtained from the integration of measured intensities.

prepared *in situ*, UHV, using repeated cycles of Ar^+ sputtering (1 kV) followed by annealing at 1100 K under UHV (base pressure 9×10^{-10} mbar). The annealing temperature was measured using an optical pyrometer with the emissivity set to 0.35. The structure quality and the cleanliness of the surface were checked by LEED and XPS, before the SXRD experiment, in a UHV chamber installed in a side laboratory. The sample was transferred using a UHV suitcase in the UHV diffractometer, and the surface was prepared again *in situ* using the same sputtering and annealing cycles (max pressure during the transfer: 1×10^{-7} mbar).

A total number of 189 crystal truncation rods (CTRs) were measured. In the following, we adopt notations commonly used in the SXRD community, i.e., z axis perpendicular to the surface. Then x_{bulk} corresponds to z, y_{bulk} to x, and z_{bulk} to y. With the new convention, the 189 measured CTRs correspond to $0 \leqslant h \leqslant 14, 0 \leqslant k \leqslant 14$, and $0.9 \leqslant \ell \leqslant 4.9$. The measured intensities were integrated and converted to structure factors $F_{hk}(\ell)$ using a python script based on Ref. [35] under the PYMCA program [36], which takes into account a whole range of correction factors [37,38]. The main diffraction peaks present in the $F_{hk}(\ell)$ were then removed in the range $\Delta\ell = \pm 0.2$ to emphasize the surface contribution. The intensities from symmetry-equivalent rods were averaged using the AVE program assuming one mirror plane inherited from the bulk structure. Indeed, intensities display a mirror symmetry, as shown in Fig. 5: $(h,k,\ell) = (-h,k,\ell)$. The final data set consists of 124 symmetry-nonequivalent CTRs, i.e., 8416 experimental points.

B. Surface x-ray diffraction: Calculations

The ANA-ROD program developed by Vlieg [39] was used to simulate the structure factors, using as a starting point for the fits the models described in Sec. II. The models have been allowed to relax, and the structures have been refined. The quality of the fits is quantified by the goodness of fit (GOF) defined by $\sqrt{\frac{1}{N-R}\sum \frac{(I_{\text{obs}}-I_{\text{calc}})^2}{\sigma^2}}$, where N is the number of data points (8416), R is the number of refined parameters ($115 \leqslant R \leqslant 172$ depending of the model

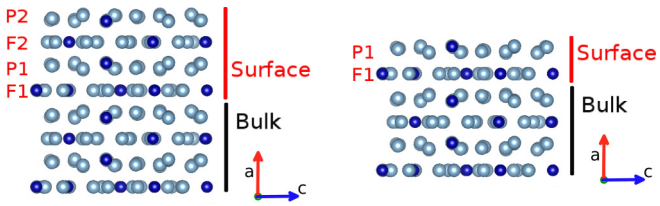

FIG. 6. Structural model implemented in the fitting process, assuming equal probability for the two possible terminations ($P1$ and $P2$).

used), and σ is the standard variation. For each surface model, the calculations have been carried out assuming equal probability for the two possible terminations (Fig. 6). The refined parameters include one scale factor, atomic positions, Debye-Waller factors, and atomic occupation numbers. To limit the number of refined parameters, the following strategy was adopted. The occupation numbers of surface atoms were fixed to 1, except for atoms positioned in the termination layer, for which six independent occupation numbers were calculated. The latter depends on the type of atom: Co^+_{bipent}, Co^-_{bipent}, Al^+_{bipent}, Al^-_{bipent}, Al^1_{glue}, and Al^2_{glue}. Here, the sign $\pm$ indicates whether the considered atomic groups are located slightly below $(-)$ or above $(+)$ the mean position of the plane (Fig. 2). The Debye-Waller factors were fixed to 0.4 for atoms positioned in the bulk, while they were refined for surface atoms. Four isotropic Debye-Waller factors were fitted: one per element for subsurface atoms, and two for Co atoms positioned in the termination layer (Co^+_{bipent}, Co^-_{bipent}). Eight anisotropic Debye-Waller factors were considered for aluminum atoms positioned in the termination layer (Al^+_{bipent}, Al^-_{bipent}, Al^1_{glue}, Al^2_{glue}). The atomic displacements were refined in three directions. Symmetry relationships were implemented for displacements of all surface and subsurface atoms. More precisely, a surface atom located in the $P1$ termination plane, with coordinates $(x_{\text{bulk}}, y_{\text{bulk}}, z_{\text{bulk}})$ using the bulk coordinate system, is supposed to have its displacements related to the ones of the corresponding surface atom located in the $P2$ termination plane with coordinates $(x_{\text{bulk}} + \frac{1}{2}, \bar{y}_{\text{bulk}}, z_{\text{bulk}} + \frac{1}{2})$. It is the same with subsurface atoms located in planes $F1$ and $F2$, respectively. Atoms located in subsubsurface planes and below were fixed at their bulk position. During the fit, each parameter was refined independently.

C. Calculations based on DFT

Complementary to the experimental study, the $Al_{13}Co_4(100)$ surface was investigated by performing calculations based on the DFT using the plane-wave Vienna *ab initio* simulation package (VASP) [40–43]. The interaction between the valence electrons and the ionic core is described using the projector-augmented-wave (PAW) method [44,45], and the calculations are performed within the generalized gradient approximation (GGA-PBE) [46,47].

The optimization of the atomic coordinates is performed via the calculation of the Hellmann-Feynman forces acting on atoms and their minimization via a conjugate gradient algorithm. Simulations of the $Al_{13}Co_4(100)$ surface are achieved by building 11-layer-thick symmetric slabs separated by a

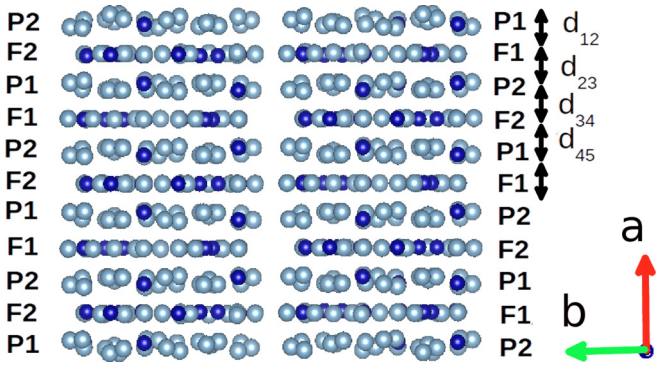

FIG. 7. Symmetric 11-layer-thick slabs used in the DFT calculations, presenting either the $P1$ or $P2$ termination

20-Å-thick vacuum region. The two possible terminations ($P1$ and $P2$) were considered (Fig. 7). The cutoff energy was set to $E_{cut} = 500$ eV, and the k-point grid was set to $5 \times 4 \times 8$ and $5 \times 4 \times 1$ for bulk and surface calculation, respectively.

IV. RESULTS

A. Comparison of the structural models by SXRD

Table I and Fig. 1 of Supplemental Material summarize the main results of the fits for the different surface models. The in-plane and out-of-plane DW factors for surface aluminum atoms belonging to bipentagonal motifs (Al^+_{bipent},Al^-_{bipent}) turn out to be very small, indicated as zero in the table, for all the models. The same is true for the isotropic DW parameters of the subsurface Co and Al atoms, except for subsurface Al atoms in the case of the P_{24}^{Al,Co^-} model (DW $Al_{subsurface} = 0.68$).

The comparison of the different models reveals an interesting indication. First, we can notice that the presence of protruding surface Co atoms is very unlikely. Indeed, the DW factor for Co^+ atoms is very large, larger than 17.5 for models containing protruding surface Co atoms ($P_{12}^{Al^-,Co^+}$, P_{24}^{Al,Co^+}), and the occupancy of protruding surface Co atoms is rather low (lower than 0.6). Either a high DW parameter value or a low occupancy have, as an effect, a reduction of the contribution of these atoms to the diffracted intensity. This means that the contribution of the protruding Co atoms is very improbable.

Distinct conclusions can be drawn when investigating the influence of buried surface Co atoms (Co^- atoms) by comparing the P_{22}^{Al} and P_{24}^{Al,Co^-} models on the one hand, and the $P_{12}^{Al^+,Co^-}$ and $P_{10}^{Al^+}$ models on the other hand. Here, parameters deduced for the fit are not drastically different with and without the presence of surface Co^- atoms. A slight improvement of the fit is observed when removing Co^- atoms from the $P_{12}^{Al^+,Co^-}$ surface, while a slight deterioration of the fit is observed when removing Co^- atoms from the P_{24}^{Al,Co^-}.

The SXRD analysis allows us to discriminate between surface models presenting identical surface chemical composition and density. This can be linked with the presence/absence of surface protruding Co atoms when comparing P_{24}^{Al,Co^-} versus P_{24}^{Al,Co^+}, or $P_{12}^{Al^-,Co^+}$ versus $P_{12}^{Al^+,Co^-}$. For incomplete models containing no surface Co atoms ($P_{10}^{Al^-}$ versus $P_{10}^{Al^+}$), the differences lie in the partial occupancies of Al surface atoms. For $P_{10}^{Al^-}$, the occupancy N_{occ} Al^- is relatively high (0.8) but the GOF is rather large (1.68), while for $P_{10}^{Al^+}$, the GOF is lower (1.57) but the Al occupancy is rather low (N_{occ} $Al^+ = 0.6$), corresponding to a very loose surface termination. In both cases, the fits are not satisfactory.

The influence of the surface density can be explored by comparing $P_{26}^{Al,Co}$ and $P_{12}^{Al,Co}$ models, for which the chemical composition of the topmost plane is similar ($\simeq$0.16 Co at. %). Fits are in favor of the denser model. Indeed, the surface Co DW factors for incomplete models are quite high: 20.0 for the model containing protruding Co atoms and 2.1 for $P_{12}^{Al^+,Co^-}$. In the latter case, the occupancy of surface Al atoms is quite low (0.5), meaning that this model is unlikely. Furthermore, the GOFs are higher for incomplete models (1.63 and 1.66) and lower (1.46) for $P_{26}^{Al,Co}$.

To summarize, fits lead to the conclusion that acceptable models are the ones presenting a dense topmost layer, without protruding surface Co atoms. These two criteria are met for both the P_{22}^{Al} and P_{24}^{Al,Co^-} models. These two models present consistent fitted parameters and low GOF values (1.48 for P_{24}^{Al,Co^-} and 1.59 for P_{22}^{Al}). It is worth noting here that the low occupancy of the surface Co^+ sites of $P_{26}^{Al,Co}$ (0.4) means that this refined surface model, which also presents a low GOF value (1.48), is very similar to P_{24}^{Al,Co^-}. For the P_{22}^{Al} model, the absence of Co^- atoms, located at the center of a pentagonal motif made of protruding Al^+ atoms, leads to a slight decrease of the occupancy for the closest Al atoms (Al^+). This is probably due to the rather strong bond linking these two types of atoms (Al^+,Co^-) in the bulk [48]. In the following, we focus on P_{24}^{Al,Co^-}, which presents one of the lowest GOFs of all the models.

TABLE I. GOF, Debye-Waller factors (DW), and occupation numbers (N_{occ}) deduced from the fitting process. DW and N_{occ} (GOF) are rounded off to one (two) decimal points.

	P_{22}^{Al}	$P_{26}^{Al,Co}$	P_{24}^{Al,Co^-}	P_{24}^{Al,Co^+}	$P_{12}^{Al^-,Co^+}$	$P_{10}^{Al^-}$	$P_{12}^{Al^+,Co^-}$	$P_{10}^{Al^+}$
GOF	1.59	1.46	1.48	1.59	1.66	1.68	1.63	1.57
DW Co^-		0.0	0.0				2.1	
DW Co^+		0.0		17.5	20.0			
N_{occ} Al^+	0.6	0.8	0.8	0.7			0.5	0.6
N_{occ} Al^-	0.9	1.0	1.0	0.9	0.8	0.8		
N_{occ} Co^-		0.9	0.6				0.9	
N_{occ} Co^+		0.4		0.6	0.6			

B. Refinement of the P_{24}^{Al,Co^-} model by SXRD

Additional experiments on the fitting procedures have been performed using the P_{24}^{Al,Co^-} model. A slight increase in the surface Co occupation number is obtained (N_{occ} $Co^- = 0.7$) when both the occupation number and the corresponding Debye-Waller factor are allowed to vary together, all other parameters remaining the same. Two additional models have also been built by removing one surface Al glue atom. They lead to a slight decrease of the GOF (from 1.48 to 1.47 and 1.46), and a small decrease of N_{occ} Co^- (N_{occ} $Co^- = 0.5, 0.6$).

TABLE II. Interlayer relaxations and corrugation of the surface planes, deduced from SXRD and DFT. See Fig. 7 for notations. Values in parentheses are bulk values.

	SXRD	DFT
r_{12}	-1.5%	-0.5%
r_{23}	$+2.1\%$	$\leq 0.1\%$
r_{34}		$+0.8\%$
r_{45}		$\leq 0.1\%$
$\Delta_P^{\text{topmost}}$	1.03 Å	0.87 Å
	(0.28 Å)	(0.65 Å)
$\Delta_F^{\text{subsurf}}$	0.49 Å	0.21 Å

The largest difference is obtained with the occupation number of this atomic position: 1.5 and 0.8 when two glue atoms are considered, while the occupancy of surface Al glue atoms is found to be lower for surface models containing only one glue atom (1.1 and 0.5, depending on the type of glue atom remaining at the surface).

In the following, we focus on the result obtained for a fit performed with the presence of two glue atoms while optimizing simultaneously the occupation number and the corresponding Debye-Waller factor (N_{occ} $\text{Co}^- = 0.7$). The interlayer distance relaxation r_{ij} between two consecutive planes i and j is calculated by $r_{ij} = \frac{d_{ij}-d_0}{d_0}$, where d_{ij} and d_0 are the interlayer distances in the surface and bulk systems, respectively. Here, we take the bulk structure determined by x-ray diffraction as the reference ($d_0 = 2.04$ Å). Similarly, the corrugation Δ_i of planes i is compared to the bulk values. Here, all atoms in the atomic layers are considered. This means that only 24 atoms are taken into account for the topmost layer, while they are 26 for buried puckered layers. Using the labels of Fig. 6, we found a contraction of the topmost layers (-1.5%), while the subsurface relaxation is an expansion ($+2.1\%$). The plane corrugation is increased at the surface compared to the bulk: $\Delta_P^{\text{topmost}} = 1.03$ Å ($\Delta_P^{\text{bulk}} = 0.28$ Å), $\Delta_F^{\text{subsurf}} = 0.49$ Å. Results are gathered in Table II, and atomic coordinates in the two topmost layers are shown in Table 1 of the Supplemental Material [49].

C. Surface structure from DFT calculations

The relaxation of the bulk structure leads to the following cell parameters: $a_{\text{bulk}} = 8.20$ Å, $b_{\text{bulk}} = 12.41$ Å, and $c_{\text{bulk}} = 14.43$ Å, in good agreement with experimental values. This leads to an interlayer distance equal to 2.05 Å, again in good agreement with the experiment (2.04 Å).

Two 11-layer-thick slabs are considered to model the $P_{24}^{\text{Al,Co}^-}$, each one presenting a given puckered termination ($P1$ or $P2$). Unlike the SXRD approach, no symmetry constraints have been applied here. After atomic relaxation, both calculations lead to the same structure, the same interlayer distance relaxations, and the same surface energy. These results support the symmetry relationships implemented in the SXRD analysis.

More precisely, the interlayer distance relaxations are gathered in Table II. The corrugation of the topmost puckered plane is found to increase at the surface compared to the bulk, as already demonstrated by SXRD results. Similar trends are found for surface relaxations on $Al_{13}Co_4(100)$, using SXRD or DFT calculations. The interlayer distance shows a contraction at the surface in both cases, while an expansion is calculated for subsurface planes (r_{34} for DFT and r_{23} for SXRD). The discrepancies observed here between SXRD and DFT are attributed to the limited number of planes (two planes) considered for relaxation in the SXRD study.

V. DISCUSSION

A. Surface structure deduced from SXRD, LEED-IV, and DFT

We have shown that the fits of the large experimental SXRD data set allow us to discriminate among various possible structure models of the complex $Al_{13}Co_4(100)$ surface. A careful investigation of the influence of the surface atomic composition and density leads to a restriction of the possible solutions to only two possible models ($P_{24}^{\text{Al,Co}^-}$ and P_{22}^{Al}). This conclusion is in good agreement with previous studies. The incomplete $P_{12}^{\text{Al}^+,\text{Co}^-}$ and $P_{10}^{\text{Al}^+}$ models are calculated to be thermodynamically unstable [25], while the incomplete models deduced from a simulated cleavage ($P_{12}^{\text{Al}^-,\text{Co}^+}$ and $P_{10}^{\text{Al}^-}$) [13], which are calculated to be thermodynamically stable for Co-rich compounds, do not correspond with the experimental STM images [25] and are not supported by our SXRD analysis. Calculations of Ref. [13] were done with the constraint of a constant number of atoms in the simulation cell, which do not correspond to the experimental approach, leading to biased results.

Our results are also compatible with those obtained via a LEED-IV analysis [25], which identified the almost complete P_{22}^{Al} model as the surface model with the lowest Pendry R-factor (0.26). Here, the disagreement between the previous LEED-IV results and the SXRD ones consists only in the presence/absence of two surface Co atoms slightly below the mean position of the plane. According to LEED-IV analysis, the Pendry R-factor of our best model ($P_{24}^{\text{Al,Co}^-}$) is 0.31, i.e., very similar to that of the P_{22}^{Al} model without a few Al glue atoms (R-factor in the range 0.29–0.32). From SXRD, taking into account the presence of two or only one glue atom ($P_{24}^{\text{Al,Co}^-}$ model) does not change drastically the GOF: it stays in the range 1.46–1.48, i.e., below the GOF of other models. Altogether, results converge toward a surface termination of the $Al_{13}Co_4(100)$ at puckered layers where protruding Co^+ atoms are missing and where the subsurface Co^- and Al glue atoms are best described with a partial occupancy.

Both SXRD and DFT calculations lead to similar trends in surface relaxation (the $P_{24}^{\text{Al,Co}^-}$ model; see Fig. 8 and Table 2 of the Supplemental Material [49]). The interlayer distance shows a contraction at the surface in both cases, while the corrugation of the topmost layer increases. The comparison of the atomic positions obtained by both methods gives very similar results. To illustrate this point, a projection of the atomic positions located in the topmost puckered plane, determined by SXRD (in blue) or DFT (in orange), is shown in Fig. 9. The differences found for the topmost atomic coordinates, by comparing the two approaches, are very small for in-plane positions (below 0.02 Å), while they are

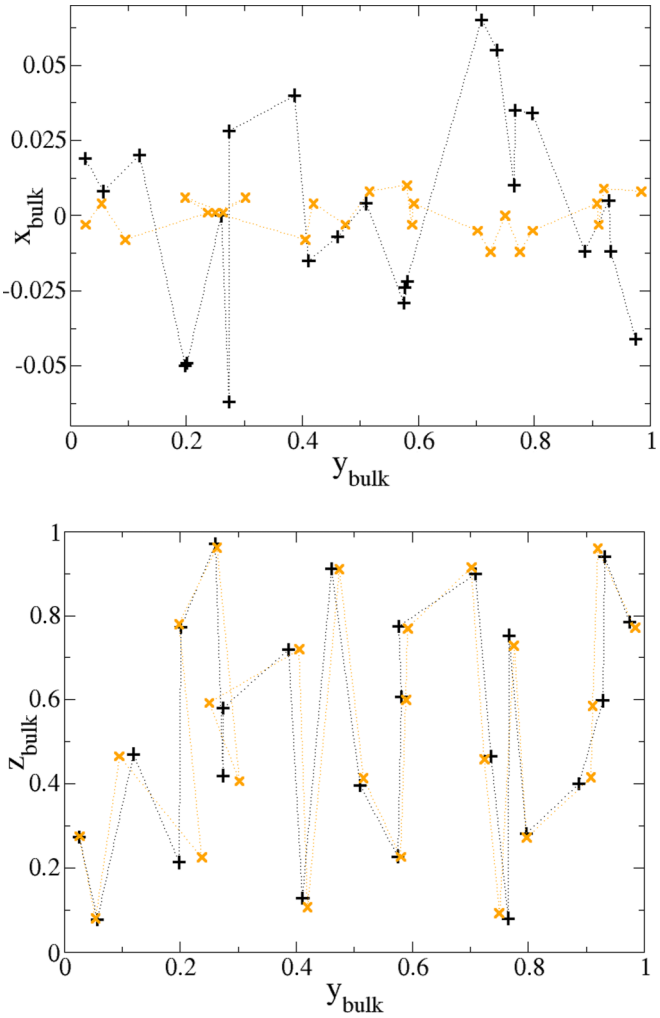

FIG. 8. Atomic relaxations deduced from SXRD (in black) and DFT (in red-orange) as a function of the y_{bulk} (or x) coordinate. Top: relaxations perpendicular to the surface plane (x_{bulk} or z). The x_{bulk} coordinate is given relatively to the mean position of the plane. Bottom: relaxations parallel to the surface plane (z_{bulk} or y).

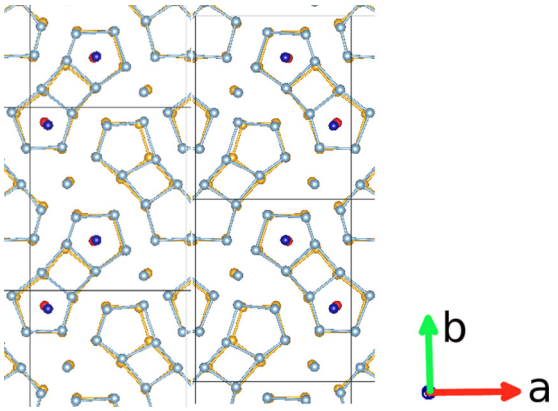

FIG. 9. Atomic relaxations deduced from SXRD (in blue) and DFT (in red-orange) of the two types of puckered surface planes (P_{24}^{Al,Co^-} model). Al (Co) atoms are shown by a light (dark) color. Only atoms in the topmost plane are represented. The surface cell is drawn by black lines.

larger for out-of-plane positions (below 0.04 Å). The quantity $[(x_{SXRD} - x_{DFT})^2 + (y_{SXRD} - y_{DFT})^2 + (z_{SXRD} - z_{DFT})^2]^{\frac{1}{2}}$ is smaller than 0.075 for surface atoms located in the topmost puckered plane.

The previous LEED-IV analysis of the $Al_{13}Co_4(100)$ surface led to different conclusions regarding surface relaxations, with an interlayer relaxation of $+1\%$ and -1% for the two surface layers of the first type (P1F2 and F2P2), while the order is reversed for the other type (i.e., -1% and $+1\%$ for P2F1 and F1P1) [25]. Such a reversal is not reproduced by the SXRD results and DFT calculations. This discrepancy may come from the assumption of a strictly ordered surface (no partial occupancies were used) and from the optimization of each termination separately, compared to the data obtained from a surface having both terminations. A better procedure would have been to optimize the two terminations simultaneously with the experimental data, like the approach adopted in the present paper. However, this was not realized due to limitations intrinsic to LEED-IV analysis of such a large system.

B. Surface energy deduced from DFT calculations

Surface energy is evaluated using the method described in Ref. [25]. While in Ref. [25] asymmetric slabs were built and relative surface energies were obtained to compare surface models, in the present paper we use symmetric slabs in order to calculate absolute surface energies.

The surface energy is calculated to be 1.09 J/m^2 when the chemical potential for Al is taken to be that of bulk aluminum (−3.50 eV). It is lower than the surface energy for the termination resulting from a simulated cleavage (Z termination in Ref. [50]), calculated to be 1.19 J/m^2. It is also lower than the calculated surface energies for the related Al_5Co_2 compound in the same Al-rich limit: 1.34 J/m^2 for (001), 1.38 J/m^2 for (100), and 1.27 J/m^2 for $(2\bar{1}0)$ surfaces.

The surface energy calculated for $Al_{13}Co_4(100)$ is larger than the calculated values for Al(111): 0.80 J/m^2 (GGA approximation [51]), 1.00 J/m^2 (LDA approximation [51]), 0.83 J/m^2 (all electron calculation, within GGA [52]). As already highlighted for the Al_5Co_2 low-index surfaces, it is substantially related to the concentration of surface Co atoms [53].

This result can be set against unusual surface properties of complex metallic phases compared to simple metals [54]. In particular, contact angles of Pb droplets on polycrystalline films of aluminum and $Al_{13}Co_4$ have been reported. On polycrystalline films of aluminum, the contact angles are measured to be around 30 degrees, while they are around 50 degrees for polycrystalline films of $Al_{13}Co_4$ [55]. If the experimental systems were effectively at thermodynamic equilibrium, the previous results would show that the interfacial energy difference $\gamma_{Pb/Al_{13}Co_4(100)} - \gamma_{Pb/Al(111)}$ is larger than the difference in surface energies $\gamma_{Al_{13}Co_4(100)} - \gamma_{Al(111)}$ ($\simeq$0.4 J/m^2). This is consistent with previous Pb thin-film growth on the same surfaces. While on Al(111) the Pb adatoms are very mobile and the film grows in a layer-by-layer fashion up to several tens of layers [56], on the $Al_{13}Co_4(100)$ surface the diffusion of Pb adatoms is much more reduced and only a single pseudomorphic layer can be grown [57] followed by the formation of large Pb mounds upon further dosing. This could

be related to the Stranski-Krastanov growth mode involving interfacial strain in the film due to lattice mismatch.

VI. CONCLUSION

This paper presents a surface structure determination by SXRD of a quasicrystalline approximant, the $Al_{13}Co_4$ phase, a complex intermetallic compound with more than 100 atoms in its unit cell. This achievement was only possible due to the large experimental data set that could be recorded—the largest experimental data set ever analyzed with SXRD—a consequence of the high density of crystal truncation rods and of the relatively low symmetry of the system (124 symmetry-nonequivalent CTRs). Fits of the SXRD data allowed us to discriminate among various surface models and pointed toward a bulk truncated surface at dense Al-rich puckered planes where protruding surface Co atoms are missing. Surface relaxations and exact atomic positions obtained by SXRD and complementary DFT calculations are very similar and give confidence in the analysis. In addition, the surface energy of the corresponding surface model could be estimated from DFT calculations with a rather low value of 1.09 J/m^2. This in turn allowed us to estimate interfacial energy differences $\gamma_{Pb/Al_{13}Co_4(100)} - \gamma_{Pb/Al(111)}$ larger than 0.4 J/m^2, consistent with a complex interface structure. This study opens up alternative perspectives for the determination of complex surface structures, such as quasicrystalline and related intermetallic surfaces.

ACKNOWLEDGMENTS

This work was supported by the ANR CAPRICE 2011-INTB 1001-01, the European C-MAC consortium. This work was made possible thanks to the HPC resources of IDRIS made available by GENCI (Grand Equipement National de Calcul Intensif) (project 99642). We acknowledge the European Synchrotron Radiation Facility for provision of synchrotron radiation facilities and we would like to thank two of us for assistance in using beamline ID03.

[1] X. L. Ma and K. H. Kuo, Metall. Trans. A **23**, 1121 (1992).
[2] J. Grin, U. Burkhardt, M. Ellner, and K. Peters, J. Alloys Compd. **206**, 243 (1994).
[3] U. Burkhardt, M. Ellner, and J. Grin, Powder Diffr. **11**, 123 (1996).
[4] F. Fleischer, T. Weber, D. Y. Jung, and W. Steurer, J. Alloys Compd. **500**, 153 (2010).
[5] P. Priputen, M. Kusý, M. Drienovský, D. Janičkovič, R. Čička, I. Černičková, and J. Janovec, J. Alloys Compd. **647**, 486 (2015).
[6] M. Mihalkovič and M. Widom, Phys. Rev. B **75**, 014207 (2007).
[7] J. Dolinsek, M. Komelj, P. Jeglic, S. Vrtnik, D. Stanic, P. Popcevic, J. Ivkov, A. Smontara, Z. Jaglicic, P. Gille, and Y. Grin, Phys. Rev. B **79**, 184201 (2009).
[8] M. Heggen, L. Houben, and M. Feuerbacher, Nat. Mater. **9**, 332 (2010).
[9] *Complex Metallic Alloys: Fundamentals and Applications*, edited by J.-M. Dubois and E. Belin-Ferré (Wiley-VCH, Weinheim, 2011).
[10] J.-M. Dubois and E. Belin-Ferré, Sci. Technol. Adv. Mater. **15**, 034804 (2014).
[11] *Surface Properties and Engineering of Complex Intermetallics*, edited by E. Belin-Ferré (World Scientific, Singapore, 2010), Vol. 3.
[12] M. Armbrüster, K. Kovnir, Y. Grin, R. Schlögl, P. Gille, M. Heggen, and M. Feuerbacher, Eur. Pat. 09157875.7 (2009).
[13] M. Krajčí and J. Hafner, J. Catal. **278**, 200 (2011).
[14] M. Armbrüster, K. Kovnir, M. Friedrich, D. Teschner, G. Wowsnick, M. Hahne, P. Gille, L. Szentmiklosi, M. Feuerbacher, M. Heggen, F. Girgsdies, D. Rosenthal, R. Schlögl, and Y. Grin, Nat. Mater. **11**, 690 (2012).
[15] M. Armbrüster, R. Schlögl, and Y. Grin, Sci. Technol. Adv. Mater. **15**, 034803 (2014).
[16] A. Michaelides and M. Scheffler, in *Surface and Interface Science. Volume 1: Concepts and Methods*, edited by K. Wandelt (Wiley, Weinheim, Germany, 2012).
[17] D. P. Woodruff, J. Phys.: Condens. Matter **22**, 084016 (2010).
[18] *Surface Alloys and Alloy Surfaces*, Vol. 10 of The Chemical Physics of Solid Surfaces, edited by D. Woodruff (Elsevier Science, Amsterdam, 2002).
[19] P. Thiel, Annu. Rev. Phys. Chem. **59**, 129 (2008).
[20] J. Ledieu, É. Gaudry, and V. Fournée, Sci. Technol. Adv. Mater. **15**, 034802 (2014).
[21] P. Gille and B. Bauer, Cryst. Res. Technol. **43**, 1161 (2008).
[22] C. L. Henley, J. Non-Cryst. Solids **153-154**, 172 (1993).
[23] P. Jeglic, S. Vrtnik, M. Bobnar, M. Klanjsek, B. Bauer, P. Gille, Y. Grin, F. Haarmann, and J. Dolinsek, Phys. Rev. B **82**, 104201 (2010).
[24] R. Addou, É. Gaudry, T. Deniozou, M. Heggen, M. Feuerbacher, P. Gille, Y. Grin, R. Widmer, O. Gröning, V. Fournée, J.-M. Dubois, and J. Ledieu, Phys. Rev. B **80**, 014203 (2009).
[25] H. Shin, K. Pussi, É. Gaudry, J. Ledieu, V. Fournée, S. Alarcón Villaseca, J.-M. Dubois, Yu. Grin, P. Gille, W. Moritz, and R. D. Diehl, Phys. Rev. B **84**, 085411 (2011).
[26] V. Fournée, É. Gaudry, M.-C. de Weerd, R. D. Diehl, and J. Ledieu, Complex Metallic Alloys. Mater. Res. Soc. Symp. Proc. **1517** (2012).
[27] M. V. Hove, W. Moritz, P. J. Rous, A. Wander, A. Barbieri, N. Materer, U. Starke, and G. A. Somorjai, in *Automated Determination of Complex Surface Structures by LEED*, Tutorials on Selected Topics in Modem Surface Science, edited by T. Barr and D. Saldin (Elsevier Science, Amsterdam, 1993).
[28] M. Van Hove, W. Weinberg, and C. Chan, *Low-Energy Electron Diffraction: Experiment, Theory and Surface Structure Determination*, Springer Series in Surface Sciences (Springer, Berlin, 2012).
[29] R. Feidenhans'l, Surf. Sci. Rep. **10**, 105 (1989).
[30] I. K. Robinson and D. J. Tweet, Rep. Prog. Phys. **55**, 599 (1992).
[31] E. Vlieg, J. F. Van Der Veen, S. J. Gurman, C. Norris, and J. E. Macdonald, Surf. Sci. **210**, 301 (1989).

[32] M. Capitan, Y. Calvayrac, D. Gratias, and J. Alvarez, Physica B **283**, 79 (2000).
[33] X. Torrelles, M. Pedio, C. Cepek, and R. Felici, Phys. Rev. B **86**, 075461 (2012).
[34] O. Balmes, R. van Rijn, D. Wermeille, A. Resta, L. Petit, H. Isern, T. Dufrane, and R. Felici, Catal. Today **145**, 220 (2009).
[35] J. Drnec, T. Zhou, S. Pintea, W. Onderwaater, E. Vlieg, G. Renaud, and R. Felici, J. Appl. Crystallogr. **47**, 365 (2014).
[36] V. Solé, E. Papillon, M. Cotte, Ph. Walter, and J. Susini, Spectrochim. Acta Pt. B **62**, 63 (2007).
[37] E. Vlieg, J. Appl. Crystallogr. **30**, 532 (1997).
[38] E. Vlieg, J. Appl. Crystallogr. **31**, 198 (1998).
[39] E. Vlieg, J. Appl. Crystallogr. **33**, 401 (2000).
[40] G. Kresse and J. Hafner, Phys. Rev. B **47**, 558 (1993).
[41] G. Kresse and J. Hafner, Phys. Rev. B **49**, 14251 (1994).
[42] G. Kresse and J. Furthmüller, Phys. Rev. B **54**, 11169 (1996).
[43] G. Kresse and J. Furthmüller, Comput. Mater. Sci. **6**, 15 (1996).
[44] P. E. Blöchl, Phys. Rev. B **50**, 17953 (1994).
[45] G. Kresse and D. Joubert, Phys. Rev. B **59**, 1758 (1999).
[46] J. P. Perdew, K. Burke, and M. Ernzerhof, Phys. Rev. Lett. **77**, 3865 (1996).
[47] J. P. Perdew, K. Burke, and M. Ernzerhof, Phys. Rev. Lett. **78**, 1396 (1997).
[48] M. Armbrüster, K. Kovnir, Y. Grin, and R. Schlögl, in *Complex Metallic Phases in Catalysis*, Complex Metallic Alloys, edited by J.-M. Dubois and E. Belin Ferré (Wiley, Germany, 2011).
[49] See Supplemental Material at http://link.aps.org/supplemental/10.1103/PhysRevB.94.165406 for the atomic coordinates in the two topmost layers (Table 1), the comparison of atomic relaxations deduced from SXRD and DFT (Table 2) and for the comparison between the experimental and fitted SXRD data (Fig. 1).
[50] M. Krajčí and J. Hafner, Phys. Rev. B **84**, 115410 (2011).
[51] A. Benali, C. Lacaze-Dufaure, and J. Morillo, Surf. Sci. **605**, 341 (2011).
[52] J. L. F. DaSilva, Phys. Rev. B **71**, 195416 (2005).
[53] M. Meier, J. Ledieu, M.-C. De Weerd, V. Fournée, and É. Gaudry, Phys. Rev. B **93**, 075412 (2016).
[54] J.-M. Dubois, *Useful Quasicrystals* (World Scientific, Singapore, 2005).
[55] C. Bergman, Ch. Girardeaux, C. Perrin-Pellegrino, P. Gas, J.-M. Dubois, and N. Rivier, J. Phys.: Condens. Matter **20**, 314010 (2008).
[56] T. Deniozou, J. Ledieu, V. Fournée, D. M. Wu, T. A. Lograsso, H. I. Li, and R. D. Diehl, Phys. Rev. B **79**, 245405 (2009).
[57] R. Addou, A. K. Shukla, S. Alarcón Villaseca, É. Gaudry, Th. Deniozou, M. Heggen, M. Feuerbacher, R. Widmer, O. Gröning, V. Fournée, J.-M. Dubois, and J. Ledieu, New J. Phys. **13**, 103011 (2011).